Mechanical Properties and Fracture Characteristics of Zr-Based Bulk Metallic Glass Composites Containing Carbon Nanotube Addition

doi: 10.1557/JMR.2004.0140

Mechanical properties and fracture characteristics of Zr-based bulk metallic glass composites containing carbon nanotube addition

Zan Bian,[a] Tao Zhang, Hidemi Kato, Masashi Hasegawa, and Akihisa Inoue
Institute for Materials Research, Tohoku University, Sendai 980-8577, Japan

(Received 20 August 2003; accepted 18 December 2003)

Mechanical properties and fracture characteristics of Zr-based bulk metallic glass (BMG) composites containing carbon nanotube (CNT) addition were investigated in detail. The interfacial reaction between the added CNTs and the glass matrix causes the formation of some V-shape nicks on the residual CNTs. These nicks have significant effect on the mechanical properties and fracture modes of the BMG composites. The compressive fracture strength increases with increasing the volume fraction of CNT addition at first, and starts to decrease gradually when the volume fraction of CNT addition is more than 5.0%. The fracture modes of the BMG composites also change from typical shear flow deformation behavior to completely embrittling fracture gradually. The V-shape nicks originating from the interfacial reaction are responsible for the decrease of fracture strength and the variation of fracture modes.

I. INTRODUCTION

Recently, considerable scientific and industrial effort has been made to produce bulk metallic glass (BMG) composites as a way to improve further mechanical properties compared to monolithic BMGs. BMGs are also promising matrix materials for producing composites because of their low melting points of around 1000 K and their high resistance against heterogeneous nucleation of crystals.[1,2] BMG composites reinforced with metals or ceramics particles[3–7] can improve significantly fracture strength and plasticity of Zr-based BMGs. Kato et al.[6] have reported that $Zr_{55}Al_{10}Ni_5Cu_{30}$ BMG composites containing up to 17 vol% ZrC particles were produced. The average particle size and interparticle spacing of the ZrC particles are 3 and 4 μm, respectively, and neither distinct agglomeration nor segregation of the ZrC particles is seen on the transverse and longitudinal cross-sections. The Young's modulus, compressive strength, and Vickers hardness for the composites increase almost linearly with increasing the volume fraction of ZrC from 0 to 17 vol%. The plastic elongation also increases from nearly zero for 0 vol% to 0.5% at 10 vol%. Conner et al.[3] have reported that the compressive strain of BMG composites reinforced by W, WC, Ta, and SiC increases by more than 300% compared with the unreinforced BMG, and the fracture energy of the tensile samples increases by more than 50%. Kim et al.[8] have also reported that carbon-fiber–reinforced BMG composites are prepared successfully by infiltrating liquid Zr–Ti–Cu–Ni–Be into carbon-fiber bundles. The glassy state of the matrix was retained after processing. More recently, Zr-based BMG composites containing carbon nanotubes (CNTs) were also successfully prepared.[9–11] Investigation shows that Zr-based BMG composites containing CNTs have strong ultrasonic attenuation and excellent wave absorption ability.[10,11] Residual CNTs dispersing in the glass matrix still partially keep their cylindrical graphitic structure and unique multiwalled structure.[9,11] However, up to now, the effect of CNT addition on mechanical properties of Zr-based BMG has not been investigated. The strengthening and embrittlment mechanisms of CNT addition on Zr-based BMG composites are not clarified. If BMG composites containing CNT additions still keep good mechanical properties like monolithic BMGs, this will promote greatly its potential application in some special fields. In this paper, we will investigate in detail the mechanical properties and fracture characteristic of Zr-based BMG composites containing different volume fractions of CNT addition. It is useful to develop new BMG composites in the future.

II. EXPERIMENTAL

Ingots with a nominal composition of $Zr_{52.5}Cu_{17.9}Ni_{14.6}Al_{10}Ti_5$ were prepared by arc-melting a

[a]Address all correspondence to this author.
e-mail: zanbian@imr.edu
DOI: 10.1557/JMR.2004.0140

mixture of high-purity Zr, Al, Ni, Cu, and Ti under a Ti-gettered purified Ar atmosphere. The prealloyed ingots were broken into small parts and ground mechanically into fine powder with the particle size of about 200 μm. The CNT powder with a density of 1.8 g/cm^3 was cleaned in acetone and dehydrated at 473 K. The ingot powder was mixed homogeneously with different volume fractions of CNT powder and dried immediately in a vacuum furnace for 5 h. The mixed powder was compressed into cylinders in steel dies. The cylinders were rapidly melted in a quartz tube by induction under a highly pure Ar atmosphere and then quickly cast into a copper mold by applying an argon gas pressure to produce the BMG composite rods with diameters up to 2~3 mm. X-ray patterns of the BMG composites containing different volume fractions of CNT addition were analyzed by using a MAC M03 XHF diffractometer with Cu Kα radiation. The composite sample was broken into small parts and mixed with CH_3CH_2OH and then mechanically ground into very fine powder. The thin powder was put on the copper grid covered with carbon thin film, and also observed by using high-resolution transmission electron microscopy (HRTEM) in a JEM-200cx operating at 200 kV. The composite rods were cut into cylinders with length 5.1~5.3 mm, and their ends were carefully polished flat and parallel. The mechanical properties in a compressive deformation behavior were measured at a strain rate of 10^{-4} s^{-1} by using an Instron-type testing machine at room temperature. The fracture characteristics of the BMG composites were investigated by using scanning electron microcopy (SEM).

III. RESULTS

Typical x-ray diffraction (XRD) patterns of Zr-based BMG composites containing different volume fractions of CNT addition are shown in Refs. 9 and 11. It has been confirmed that the BMG composites have the mixed structure of residual CNTs and ZrC phase dispersing randomly in the BMG matrix. But, up to now, the interfacial structure between the added CNTs and the glass phase is not clear. Figure 1 shows typical transmission electron microscope morphology of residual CNTs dispersing in the BMG matrix. CNTs still keep their cylindrical carbon structure. Figure 1(b) is the enlarged images of region A in Fig. 1(a). From Fig. 1(b), one can notice that some V-shape nicks originating from the interfacial reaction between the CNTs, and the glass phase can clearly be observed. On the regions among these nicks, the CNTs still keep their tubular shape and multiwalled structure, as shown in Figs. 1(b) and 1(c). Many more details are shown in Ref. 9. This result means that there are different interfacial reaction mechanisms on the different regions of a tubular CNT. On the regions where the nicks exist, the interfacial reaction is much more drastic, and the multiwalled structure of CNTs is significantly destroyed. But, on the regions where no nicks exist, CNTs still keep their tubular and multiwalled structure, suggesting that the interfacial reaction on the regions is very difficult and the reaction rate is very slow. Figure 1(d) displays the selected area diffraction pattern (SADP) of region C in Fig. 1(b). The SADP was indexed as shown in Fig. 1(e). One can see that region C in Fig. 1(b) is the mixed structure that consists of residual CNT, ZrC phase and amorphous phase. This means that the interfacial reaction still takes place on the regions where no nicks exist on the CNTs. A thin layer of ZrC phase with mean thickness of several nanometers is formed between the amorphous phase and the residual CNT. This result implies that the residual CNT is different with the as-cast one, which is surrounded by a thin layer of ZrC phase. From the above-described, one can notice that two different phenomena of the interfacial reaction are observed on the added CNTs, suggesting that the structure of CNTs themselves are different in different local regions. One may conclude that the regions where the nicks form very easily have much higher surface energy than other regions. It can be guessed that the local regions with higher surface energy may be some structural defects or other defects. These local defects originate from the processing of as-cast CNTs. As these defects have much higher energy, they are much easier to react with Zr element in the glass phase. However, in the regions where the interfacial reaction is not drastic, CNTs themselves have much more perfect structure, which displays much higher thermal stability and chemical stability. This is consistent with the properties of as-cast CNTs with perfect multiwalled structure. This phenomenon implies that the structural perfection is also very important to CNTs themselves as reinforcement.

Figure 2 shows typical compressive load–displacement curves of the BMG composites containing different volume fractions of CNT addition. It is well known that the BMG sample displays a quite classical elastic–perfectly plastic appearance, namely, predominantly elastic behavior followed by yielding and subsequent flow along shear bands up to fracture.[12–15] The maximum fracture strength for the current BMG alloy is about 1770 MPa.[12,15] For the BMG composites containing less than 5.0 vol% CNT addition [Figs. 2(a) and 2(b)], the compressive load–displacement curve is very similar to that of the undoped BMG, namely, a quite classical elastic–plastic behavior followed by yielding and subsequent flow along shear bands up to fracture. The maximum fracture stress, estimated according to equation $\delta = F_{max}/s$ (F_{max} is the maximum value of load, s is the top or bottom surface's area of cylinders), is about 1800 MPa for the BMG composites containing 1.0 vol% CNT additions and 1947 MPa for the BMG composites containing 3.0 vol% CNT additions. The values are much larger than the compressive fracture strength value of the undoped BMG.[12–14]

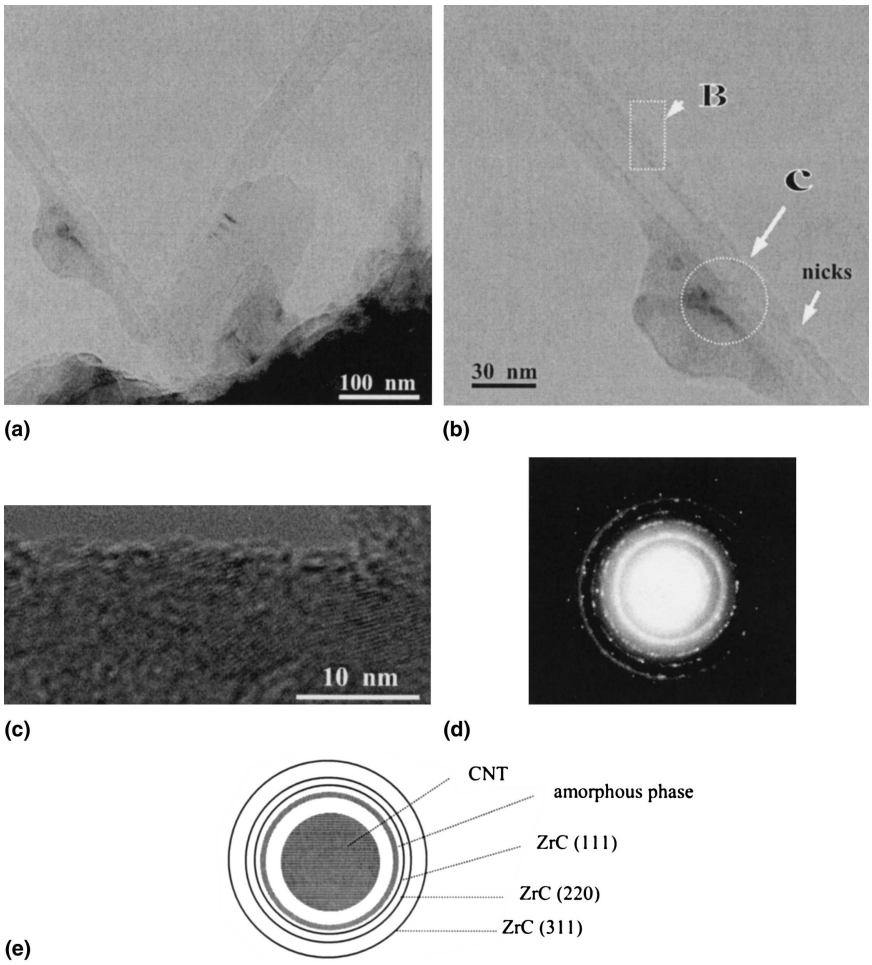

FIG. 1. TEM morphology of residual CNTs distributed into Zr-based BMG matrix. Image (a) is the typical TEM morphology of residual CNTs; image (b) is the enlarged images of region A in image (a); image (c) is an HRTEM image of region B of residual CNTs in image (b); image (d) displays the selected area diffraction pattern (SADP) of region C in image (b); and the SADP is indexed as shown in image (e).

The result implies that the addition of CNT leads to an effective dispersing strengthening. But, with further increasing the addition of CNTs (more than 5.0 vol%), the load–displacement curves [Fig. 2 (c)] show that the elastic behavior is followed by sudden fracture without presenting shear flow deformation behavior, suggesting that the BMG composites transfer to the brittle fracture. For the BMG composites containing 7.0 vol% CNT additions, its maximum fracture stress is 1873 MPa. Figure 3 exhibits the variation tendency of the maximum fracture stress of the BMG composites with increasing CNT additions. It can be noted that a strengthening tendency gradually transfers to the embrittling process with increasing CNT additions. The fracture stress of BMG composites increases with increasing CNT addition when the volume fraction of CNT addition is less than 5.0 vol%. But, with further increasing CNT addition, the BMG composites exhibit the embrittling fracture behavior. In this case, the fracture stress reduces gradually with increasing CNT additions.

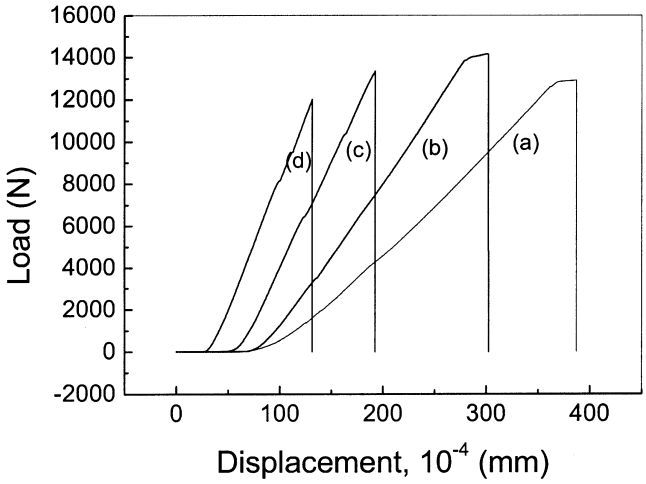

FIG. 2. Typical compressive load–displacement curves of the BMG composites containing different volume fractions of CNT addition at a strain rate of 10^{-4} s^{-1}. (a), (b), (c), and (d) are BMG composites containing 1.0, 3.0, 7.0, and 10.0 vol% CNT addition, respectively.

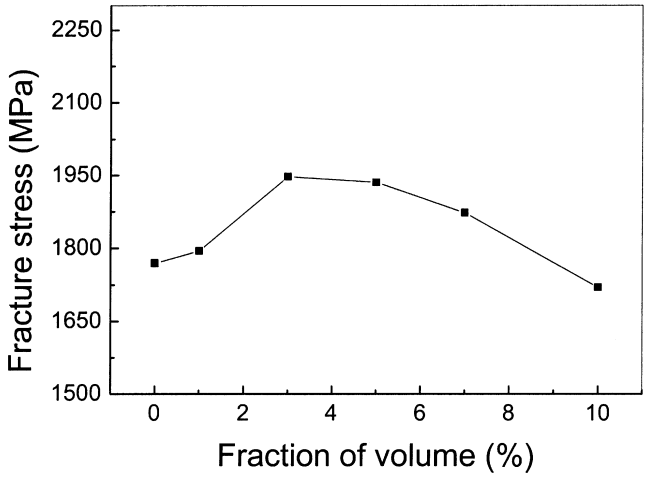

FIG. 3. The dependence of the maximum fracture stress of the BMG composites on the volume fractions of CNT addition.

Figure 4 exhibits SEM observation of fracture characteristics of the BMG composites containing 3.0 vol% CNT additions. Under uniaxial compressive loading, the fracture of the composites still occurs in a shear mode, as shown in Figs. 4(a)–4(d). The compressive fracture surface is inclined under an angle θ to the stress axis and can be measured as marked in Fig. 4(a). In agreement with the results reported on the Zr-based BMG composites or Ti-based BMG composites,[16–19] we also observe an angle of the slip plane with the compressive axis of $\theta = 41.3°$. This angle is less than 45° of most metallic glasses.[12,16,19] It implies that the random dispersion of residual CNTs in the glass matrix has an effect on the fracture behavior of BMG. From Fig. 2, the BMG composite presents typical shear flow deformation behavior. This is also supported by the fracture morphology of the composites. As shown in Fig. 4(a), the fracture surface is relatively flat and displays a typical shear fracture

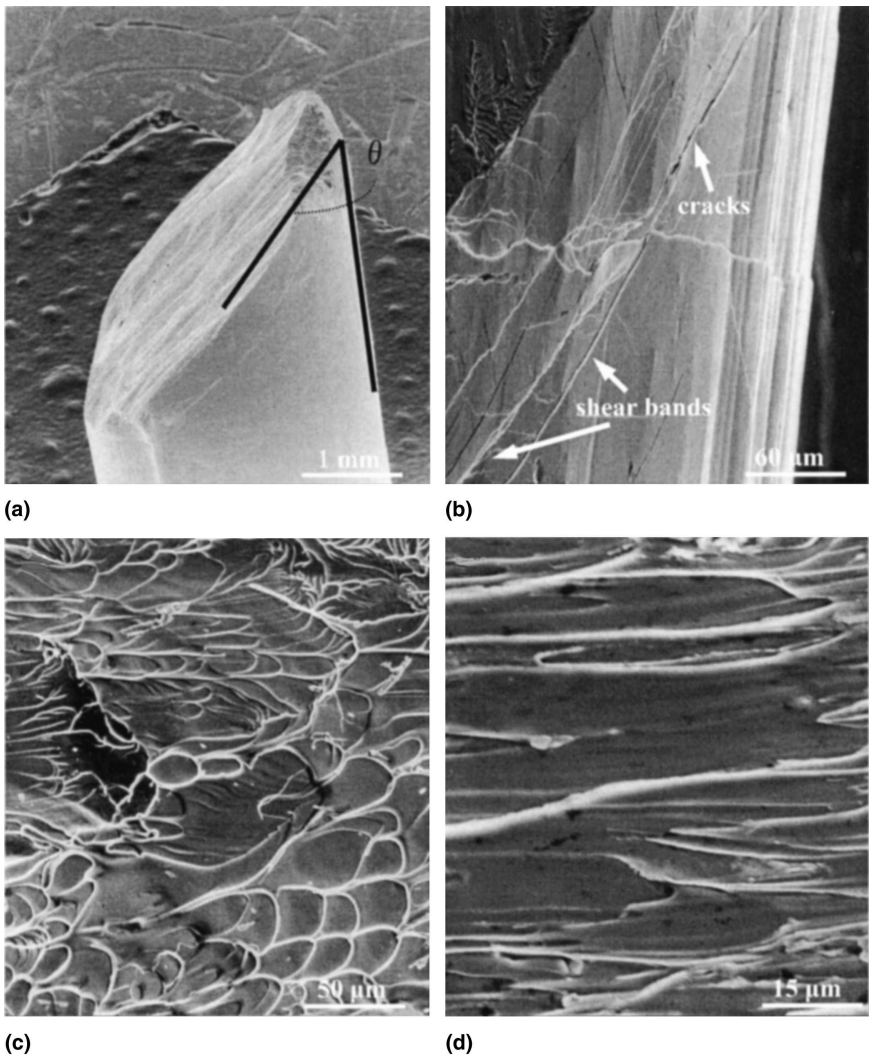

FIG. 4. Compressive fracture morphology of the BMG composites containing 3.0 vol% CNT addition. (a) Macro-appearance of the fracture surface; (b) shear bands; (c) and (d) vein patterns.

feature. SEM observation shows that the morphology of the fracture surface still exhibits the well-developed shear bands and vein-like structure as shown in Figs. 4(b) and 4(c). Shear bands with the mean spacing of about 20~25 μm are completely parallel to the shear stress direction and also consistent with the direction of fracture surface (the shear plane). The well-developed shear bands mean that drastic shear deformation has taken place under uniaxial compressive load, and the fracture behavior of the BMG composites is still governed by viscous shear deformation. This is also supported by the well-developed vein-like structure on the fracture surface. In most regions, the vein-like structure is also similar to that observed on the Zr-based BMG [shown in Fig. 4(c)]. The vein-like structure is attributed to local softening or melting within the shear bands induced by high elastic energy upon instantaneous fracture. The soft or melting metallic glass within the shear bands easily flows and appears in a vein-like structure feature. The mean size of vein patterns is about 15~20 μm, which is also similar to that of BMG.[12,14] But the other vein-pattern morphology on the fracture surface is also observed, as shown in Fig. 4(d). This vein-pattern structure is very similar to the vein patterns observed on BMG composites containing nanoscale crystals obtained by annealing.[14,15,19] It suggests that nanoscale CNTs dispersing in the glass matrix play a strengthening role similar to that of nanocrystals dispersing homogeneously in the glass matrix. From the above results, one can conclude that 3.0 vol% CNT additions do not affect significantly viscous flow deformation of the glass matrix, and the fracture of the composites is still controlled by shear flow behavior.

But the BMG composites containing more than 7.0 vol% CNT additions gradually display the embrittling fracture tendency. The fracture characteristics of the BMG composites containing 7.0 vol% CNT additions are shown in Fig. 5. Fracture surface is not flat and shows some embrittling feature. Shear bands are also observed, as shown in Fig. 5(b). The number of shear bands is little. It implies that the shear flow deformation of the composites is less than that of the BMG composites containing 3.0 vol% CNT additions. Further SEM observation displays a mixture of the vein-like structure regions and the embrittling regions on most regions of the fracture morphology, as shown in Fig. 5(c). On the vein-like structure regions, the morphology of fracture surface for the BMG composite still exhibits the vein pattern typical for the deformation of BMG alloys, but the size decrease from about 20 μm for the BMG or BMG composite containing less than 3.0 vol% CNT addition to 5~8 μm for the current composite [shown in Fig. 5(c)], which is the qualitative implication for a reduced viscous deformation in shear bands in the latter samples. But on the embrittling regions, no vein-like structure is observed, and some brittle steps are clearly displayed. One can also notice that there exist some microcracks on both regions. Several cracks cross the vein-like structure; other cracks distribute in the interfacial regions between the vein-like regions and the embrittling regions. It is possible that the microcracks initiate in the embrittling regions and cross the vein-like regions under compressive load and lead to the embrittling tendency. It means that the current composite is the mixed fracture mode including shear flow behavior and embrittling fracture behavior. The viscous shear deformation is governed by the amorphous phase, but the embrittling fracture behavior is dominated by the initiation and propagation of the microcracks. From the above description, one can conclude that the increase in CNT addition induces the embrittling tendency of the BMG composites. From XRD patterns, only ZrC phase precipitates during the interfacial reaction. The microstructure of BMG composites containing different volume fractions of CNT addition consists of CNTs and ZrC phase dispersing in the glass matrix. From the observation of the interfacial structure, the main difference is that the increase in CNT addition leads to increasing the probability of the formation of the nicks and the precipitation of ZrC phase. Kato has reported that the dispersion of ZrC phase in the glass matrix results in improving the plasticity of BMG composites.[16] Thus, the embrittlement of the BMG composites should be due to the increase of the V-shape nicks on the residual CNTs. The significant increase in the total number of the nicks per unit volume will greatly raise the probability of the nucleation and propagation of microcracks.

That the increase of CNT addition induces the embrittlement is also supported by the fracture characteristics of the BMG composites containing 10.0 vol% CNT additions, as shown in Fig. 6. The fracture surface is almost perpendicular to the applying compressive load and displays typical brittle fracture [Fig. 6(a)]. It suggests that the viscous shear deformation governed by the glass phase is not the dominant fracture mode for the current composites. On the fracture surface, there exist large amounts of brittle steps and cracks. No shear bands can be observed [Fig. 6(b)]. Further observation shows that large amounts of microcracks distribute on the fracture surface [Fig. 6(c)]. It implies that the nucleation and propagation of cracks dominates the fracture behavior of the BMG composite.

IV. DISCUSSION

The addition of CNTs forms the mixed structure of residual CNTs and ZrC phase dispersing randomly in the BMG matrix.[9,11] When a little volume fraction of CNT addition is added into the BMG matrix, the fracture behavior of the BMG composites is still governed by shear flow deformation behavior. It is confirmed by the

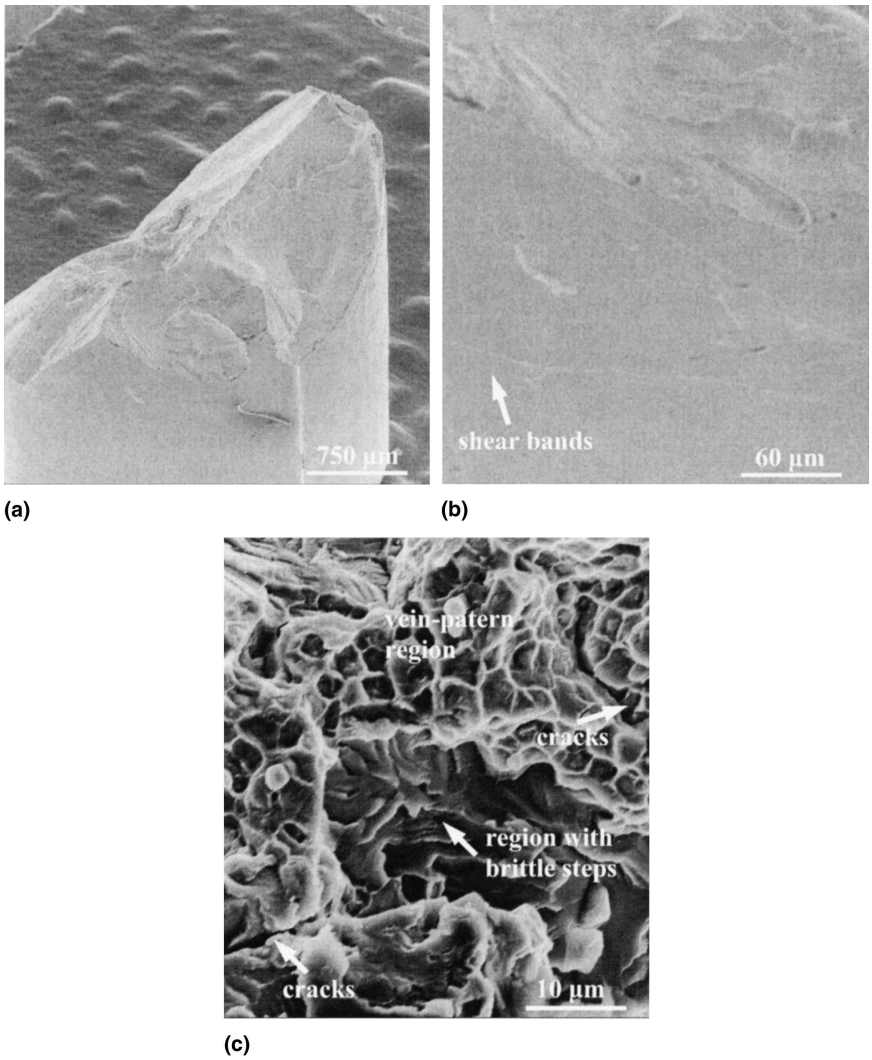

FIG. 5. Compressive fracture morphology of the BMG composites containing 7.0 vol% CNT addition. (a) Macro-appearance of the fracture surface; (b) shear bands; and (c) vein-pattern regions, brittle regions, and cracks.

load–displacement curves (shown in Fig. 2) and the fracture feature (shown in Fig. 4). During compressive deformation, nanoscale CNTs dispersing randomly in the glass matrix are an obstacle to shear flow deformation of the glass matrix and play an effective dispersing strengthening role. This is the main reason for the increase of the compressive fracture strength. When large amounts of CNTs are added into the BMG matrix (more than 5.0 vol%), the increase in the volume fraction of ZrC precipitates causes a significant depletion of Zr in the matrix.[8,9] This changes the composition of the amorphous matrix and affects the fracture strength of the composites. On the other hand, the increase in CNT addition leads to increasing the volume fraction of residual CNTs dispersing in the amorphous matrix. From Fig. 1, one can notice that large amounts of the V-shape nicks forming in the interfacial reaction between the added CNTs and the glass phase are observed. These nicks may act as the nuclei of microcracks and promote the nucleation and propagation of microcracks. When a little volume fraction of CNTs is added, the total number of these nicks are too little to affect drastically shear flow deformation behavior of the amorphous matrix.[12,14] In this case, the fracture behavior of BMG composites is still governed by viscous shear flow, and the dispersion of residual CNTs plays an effective strengthening role. But, when the volume fraction of CNT addition is larger (more than 5.0 vol%), the total number of these nicks may change the deformation behavior of the composites. In this case, the fracture behavior of BMG composites is not controlled by viscous shear flow of the amorphous matrix. As large amounts of V-shape nicks can act as the nuclei of microcracks preferentially under compressive load, the initiation of microcracks preferentially occurs from the nicks on the residual CNTs. The propagation model of the microcracks dominates the fracture

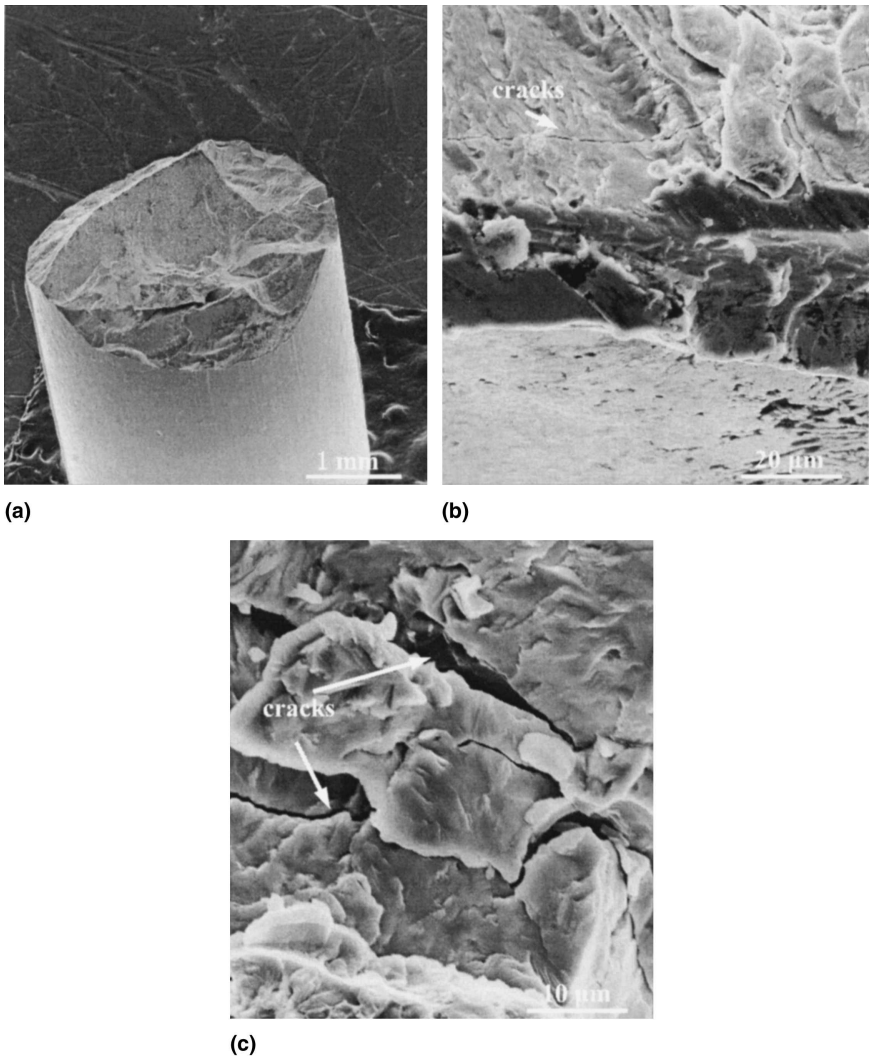

FIG. 6. Compressive fracture morphology of the BMG composites containing 10.0 vol% CNT addition. (a) Macro-appearance of the fracture surface; (b) and (c) cracks.

behavior of BMG composites. This is the reason for the embrittling fracture of BMG composites containing more than 5.0 vol% CNT additions.

Pekarskaya et al.[20] and Hays et al.[21] investigated the effect of in situ–formed ductile dendritic precipitates dispersed homogeneously in the BMG matrix on the mechanical properties, the plasticity, and the shear flow deformation of BMGs. Primary dendrite growth and solute partitioning in the molten state yields a microstructure consisting of a ductile crystalline Ti–Zr–Nb phase, with bcc structure, in a Zr-based BMG matrix. The dendritic microstructure of the Ti–Zr–Nb phase acts to seed the initiation of organized shear band patterns, confines the propagation of individual shear bands to domains having a spatial scale of the order of the primary dendrite axes length, may play a key role in initiating the formation of multiple shear bands, and leads to over 8% of total strain (elastic and plastic) of the composites.[21] He et al.[22] also reported mechanical properties of Ti-based BMG composites. The ductile dendritic hcp-Ti solid solution dispersing in the glass matrix also increases the plasticity of BMG composites. The soft dendritic network embedded in hard glass phase acts to seed the initiation of shear bands, and absorbs, redistributes, and stops the excessive localized deformation. This behavior is very similar to the results reported by Pekarskaya and Hays on the Zr-based BMG composites. BMG composites containing CNT addition have a structure similar to both above-described composites and which consists of residual CNTs with a mean length of 5~10 μm[9] and ZrC phase dispersing in the glass matrix. However, as shown in Fig. 2, BMG composites containing CNT addition become brittle with increasing the volume fraction of CNT addition. Kato has reported that ZrC crystalline dispersing in the BMG matrix also increase the plasticity of BMG composites.[6] Conner also reported similar results.[3]

The added CNTs with a mean length of about 5~10 μm also can act to seed the initiation of shear bands. However, the composites do not display the large plasticity that we expect. CNTs have extremely high elastic modulus (about 1.8 TPa)[23,24] and are one of the stiffest structures ever made. It means that residual CNTs disperse in the BMG matrix as hard sites. This is completely different with the in situ–formed ductile dendritic precipitates in both of the above composites. The hard sites embedded in the glass matrix easily induce the stress intensity between the sites and the glass matrix[12,14,15] and promote the nucleation and propagation of the microcracks.[14] Moreover, large amounts of nicks formed in the interfacial reaction are also the potential crack sources. Much more CNT additions mean that the total number of hard sites raise, suggesting that induces much stronger stress intensity. This also accelerates the nucleation and propagation of microcracks from the V-shape nicks. The combination of the stress intensity and the preferential crack from the nicks leads to the embrittlement of the composites.

V. CONCLUSIONS

In conclusion, the interfacial structure, mechanical properties, and fracture characteristics of BMG composites containing CNT addition were investigated in detail. The following conclusions are made:

(1) The interfacial reaction mechanism between the added CNTs and the glass matrix is different in different local regions of a tubular CNT. On that region where there exist some defects on the CNTs, the interfacial reaction is very drastic. The unique multiwalled structure of CNTs is significantly destroyed, and large amounts of V-shape nicks are formed. On that region where no defects exist, the interfacial reaction is slow and difficult. In this case, the interface has the mixing structure consisting of the glass phase, the thin ZrC layer, and residual CNTs.

(2) The unique interfacial structure of BMG composites containing CNT addition has a significant effect on the mechanical properties of BMG composites. The compressive fracture strength of BMG composites increases with increasing CNT addition at first, and starts to decrease gradually when the volume fraction of CNT addition is more than 5.0%.

(3) A little volume fraction of CNT addition (less than 5.0 vol%) cannot destroy shear flow deformation behavior of the amorphous matrix. The fracture behavior of BMG composites is still dominated by viscous shear flow behavior. The random distribution of residual CNTs and ZrC phase in the amorphous matrix has an effective dispersing strengthening role. For BMG composites containing more than 5.0 vol% CNT addition, the nucleation and propagation of microcracks originating from the nicks on the residual CNTs govern the fracture behavior of the composites. In this case, BMG composites display the embrittling tendency and the reducing fracture strength with increasing CNT addition.

REFERENCES

1. A. Inoue, in *Bulk Amorphous Alloys* (Materials Science Foundation, Trans Tech Publications, Zurich, 1998 and 1999) pp. 60–85.
2. W.L. Johnson, Bulk glass-forming metallic alloys: Science and Technology, MRS Bull. **24,** 42 (1999).
3. R.D. Conner, H. Choi-Yim, and W.L. Johnson, Mechanical properties of $Zr_{57}Nb_5Al_{10}Cu_5Ni_{26}$ metallic glass matrix particulate composites, J. Mater. Res. **14,** 3292 (1999).
4. R.B. Dandliker, R.D. Conner, and W.L. Johnson, Melt infiltration casting of bulk metallic-glass matrix composites, J. Mater. Res. **13,** 2896 (1998).
5. H. Choi Yim and W.L. Johnson, Bulk metallic glass matrix composites, Appl. Phys. Lett. **71,** 3808 (1997).
6. H. Kato and A. Inoue, Synthesis and mechanical properties of bulk amorphous Zr-Al-Ni-Cu alloys containing ZrC particles, Mater. Trans. JIM **38,** 793 (1997).
7. W.H. Wang and Q. Wei, Enhanced thermal stability and microhardness in Zr–Ti–Cu–Ni–Be bulk amorphous alloy by carbon addition, Appl. Phys. Lett. **71,** 58 (1997).
8. C.P. Kim, R. Bush, A. Masuhr, H. Choi-Yim, and W.L. Johnson, Processing of carbon-fiber-reinforced $Zr_{41.2}Ti_{13.8}Cu_{12.5}Ni_{10.0}Be_{22.5}$ bulk metallic glass composites, Appl. Phys. Lett. **79,** 1456 (2001).
9. Z. Bian, M.X. Pan, Y. Zhang, and W.H. Wang, Carbon-nanotube-reinforced $Zr_{52.5}Cu_{17.9}Ni_{14.6}Al_{l0}Ti_5$ bulk metallic glass composites, Appl. Phys. Lett. **81,** 4739 (2002).
10. Z. Bian, R.J. Wang, D.Q. Zhao, M.X. Pan, Z.X. Wang, and W.H. Wang, Excellent ultrasonic absorption ability of carbon-nanotube-reinforced bulk metallic glass composites, Appl. Phys. Lett. **82,** 2790 (2003).
11. Z. Bian, R.J. Wang, D.Q. Zhao, M.X. Pan, and W.H. Wang, Excellent wave absorption by zirconium-based bulk metallic glass composites containing carbon nanotubes, Adv. Mater. **15,** 616 (2003).
12. Z. Bian, G.L. Chen, G. He, and X.D. Hui, Microstructure and ductile-brittle transition of as-cast Zr-based bulk glass alloys under compressive testing, Mater. Sci. Eng. A **316,** 135 (2001).
13. R. Doglione, S. Spriano, and L. Battezzati, Static mechanical characterization of a bulk amorphous and nanocrystalline $Zr_{40}Ti_{14}Ni_{11}Cu_{10}Be_{25}$ alloy, Nanostruct. Mater. **8,** 447 (1997).
14. A. Leohard, L.Q. Xing, M. Heilmaier, A. Gebert, J. Eckert, and L. Schultz, Effect of crystalline precipitations on the mechanical behavior of bulk glass forming Zr-based alloys, Nanostruct. Mater. **10,** 805 (1998).
15. Z. Bian, G. He, and G.L. Chen, Investigation of shear bands under compressive testing for Zr-base bulk metallic glasses containing nanocrystals, Scr. Mater. **46,** 407 (2002).
16. P.E. Donovan, A yield criterion for $Pd_{40}Ni_{40}P_{20}$ metallic glass, Acta Mater. **37,** 445 (1989).
17. P. Lowhaphandu, S.L. Montgomery, and J.J. Lewandowski, Effects of superimposed hydrostatic pressure on flow and fracture of a Zr-Ti-Ni-Cu-Be bulk amorphous alloy, Scr. Mater. **41,** 19 (1999).
18. W.J. Wright, R. Saha, and W.D. Nix, Deformation mechanisms of the $Zr_{40}Ti_{14}Ni_{10}Cu_{12}Be_{24}$ bulk metallic glass, Mater. Trans. Jim. **42,** 642 (2001).
19. G. He, Z.F. Zhou, W. Loeser, J. Eckert, and L. Schultz, Effect of Ta on glass formation, thermal stability and mechanical properties of a $Zr_{52.25}Cu_{28.5}Ni_{4.75}A_{19.5}Ta_5$ bulk metallic glass, Acta Mater. **51,** 2383 (2003).

20. E. Pekarskaya, C.P. Kim, and W.L. Johnson, In situ transmission electron microscopy studies of shear bands in a bulk metallic based composites, J. Mater. Res. **16,** 2513 (2001).
21. C.C. Hays, C.P. Kim, and W.L. Johnson, Microstructure controlled shear band pattern formation and enhanced plasticity of bulk metallic glasses containing in situ formed ductile phase dendrite dispersions, Phys. Rev. Lett. **84,** 2901 (2000).
22. G. He, J. Eckert, and W. Loeser, Stability, phase transformation and deformation behavior of Ti-base metallic glass and composites, Acta Mater. **51,** 1621 (2003).
23. M.M. Trancy, T.W. Ebbesen, and J.M. Gibson, Exceptionally high Young's modulus observed for individual carbon nanotubes, Nature **381,** 678 (1996).
24. E.W. Wong, P.E. Sheehan, and C.M. Gibson, Toughness of nanorods and nanotubes, Science **277,** 1971 (1997).